HHS Public Access

Author manuscript

Cell Rep. Author manuscript; available in PMC 2018 September 24.

Published in final edited form as:

Cell Rep. 2018 August 28; 24(9): 2248–2260. doi:10.1016/j.celrep.2018.07.081.

Pathogenic TFG Mutations Underlying Hereditary Spastic Paraplegia Impair Secretory Protein Trafficking and Axon Fasciculation

Erin L. Slosarek[#1], **Amber L. Schuh**[#1], **Iryna Pustova**[#1], **Adam Johnson**[1], **Jennifer Bird**[1], **Matthew Johnson**[2], **E.B. Frankel**[1], **Nilakshee Bhattacharya**[2], **Michael G. Hanna**[1], **Jordan E. Burke**[3], **David A. Ruhl**[4], **Kyle Quinney**[1], **Samuel Block**[1], **Jennifer L. Peotter**[1], **Edwin R Chapman**[4], **Michael D. Sheets**[1], **Samuel E. Butcher**[3], **Scott M. Stagg**[2], and **Anjon Audhya**[1,6,*]

[1]Department of Biomolecular Chemistry, University of Wisconsin-Madison School of Medicine and Public Health, 440 Henry Mall, Madison, WI 53706, USA

[2]Department of Chemistry and Biochemistry, Institute of Molecular Biophysics, Florida State University, 91 Chieftan Way, Tallahassee, FL 32306, USA

[3]Department of Biochemistry, University of Wisconsin-Madison, Madison, WI 53706, USA

[4]Howard Hughes Medical Institute and Department of Neuroscience, University of Wisconsin-Madison, Madison, WI 53705, USA

[6]Lead Contact

[#] These authors contributed equally to this work.

SUMMARY

Length-dependent axonopathy of the corticospinal tract causes lower limb spasticity and is characteristic of several neurological disorders, including hereditary spastic paraplegia (HSP) and amyotrophic lateral sclerosis. Mutations in Trk-fused gene (TFG) have been implicated in both diseases, but the pathomechanisms by which these alterations cause neuropathy remain unclear. Here, we biochemically and genetically define the impact of a mutation within the TFG coiled-coil domain, which underlies earlyonset forms of HSP. We find that the TFG (p.R106C) mutation alters compaction of TFG ring complexes, which play a critical role in the export of cargoes from the endoplasmic reticulum (ER). Using CRISPR-mediated genome editing, we engineered human stem cells that express the mutant form of TFG at endogenous levels and identified specific defects

[*]Correspondence: audhya@wisc.edu.

AUTHOR CONTRIBUTIONS

E.L.S., A.L.S., I.P., A.J., M.J., S.M.S., and A.A. designed research. E.L.S., A.L.S., I.P., A.J., J.B., M.J., E.B.F., N.B., M.G.H., J.E.B., D.A.R., K.Q., S.B., J.L.P., M.D.S., S.M.S., and A.A. performed research. E.L.S., A.L.S., I.P., A.J., M.J., E.B.F., D.A.R., E.R.C., S.E.B., S.M.S., and A.A. contributed new reagents/analytic tools. E.L.S., A.L.S., I.P., A.J., M.J., E.B.F., D.A.R., S.B., S.M.S., and A.A. analyzed data. A.A. wrote the paper.

DECLARATION OF INTERESTS

The authors declare no competing interests.

SUPPLEMENTAL INFORMATION

Supplemental Information includes Supplemental Experimental Procedures and seven figures and can be found with this article online at https://doi.org/10.1016/j.celrep.2018.07.081.

in secretion from the ER and axon fasciculation following neuronal differentiation. Together, our data highlight a key role for TFG-mediated protein transport in the pathogenesis of HSP.

In Brief

Slosarek et al. demonstrate that pathological mutations in TFG, which underlie various forms of neurodegenerative disease, impair secretory protein transport from the endoplasmic reticulum and compromise the ability of axons to self-associate. These findings highlight a critical function for the early secretory pathway in neuronal maintenance.

Graphical Abstract

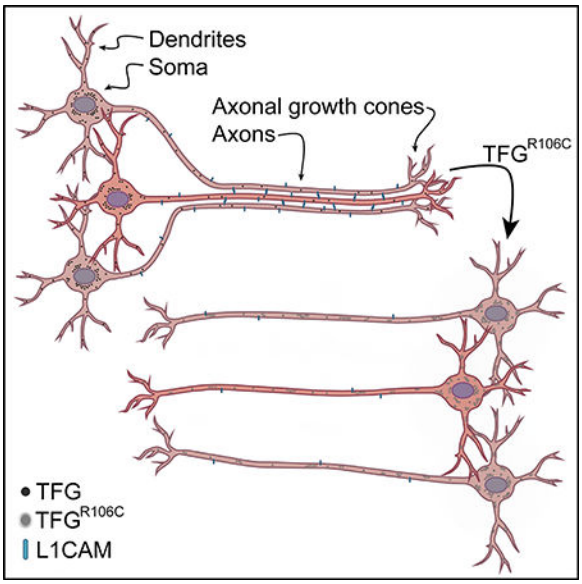

INTRODUCTION

The pyramidal motor system in humans directs voluntary movement. In particular, long cortical neurons that extend from layer V of the cerebral cortex into the spinal cord enable skilled limb mobility (Blackstone, 2012). The maintenance of these corticospinal neurons depends heavily on axonal transport of proteins, lipids, organelles, and other vesicular carriers. Thus, it is perhaps unsurprising that numerous regulators of membrane trafficking and organelle dynamics have been implicated in neurodegenerative disease (Wang et al., 2014; Saheki and De Camilli, 2017). Among inherited neuropathies, hereditary spastic paraplegias (HSPs) and hereditary motor and sensory neuropathies (HMSNs) are the most common, collectively affecting hundreds of thousands of individuals worldwide (de Souza et al., 2017; Weis et al., 2017). Despite their prevalence and severity, specific pathomechanisms underlying most of these disorders remain unknown. Nevertheless, the genetic diversity of HSPs provides an opportunity to delineate biochemical pathways that contribute to lifelong axon function.

With recent advances in whole-genome and exome sequencing technologies, there has been a surge in the identification of mutations that contribute to the development of peripheral

neuropathies. Using this approach, we and others have demonstrated that point mutations in tropomyosin receptor kinase fused gene (TFG) (also known as SPG57) contribute to the pathology of HSPs, HMSNs, and amyotrophic lateral sclerosis (ALS) (Ishiura et al., 2012; Beetz et al., 2013; Kawarai et al., 2013; Yagi et al., 2016). However, in none of these cases is it clear how the mutations lead to axonopathy. Based on functional and localization studies, TFG plays an important role in maintaining the integrity of the early secretory pathway (Witte et al., 2011; Johnson et al., 2015; Hanna et al., 2017; McCaughey et al., 2016). In the absence of TFG, subdomains on the endoplasmic reticulum (ER) that produce COPII-coated transport carriers separate away from ER-Golgi intermediate compartments (ERGICs), slowing the export of secretory cargoes from the ER and triggering an ER stress response (Johnson et al., 2015). Additionally, the organization of the ER is impaired following TFG depletion, as is the normal distribution of mitochondria in fibroblasts (Witte et al., 2011; Johnson et al., 2015). Recently, the effect of overexpressing a mutant form of TFG implicated in HSP (p.R106C) was assessed in cultured murine neurons, which revealed a reduction in the size of mitochondria in neurites (Harlalka et al., 2016). Together, these data suggest that the pathogenicity of the TFG (p.R106C) mutation may relate to an unidentified role in regulating mitochondrial function, although the artificial nature of overexpressing TFG or depleting it using small interfering RNAs (siRNAs) poorly simulates the disease condition.

A more physiologically relevant alternative to defining the impact of mutations in neurons has evolved with the development of stem cell technologies. Tissue samples acquired from patients are now routinely cultured and reprogrammed in vitro to generate induced pluripotent stem cells (iPSCs), which can be differentiated toward a number of distinct fates, including the telencephalic glutamatergic cortical neurons that are affected in HSP (Vazin et al., 2014; Denton et al., 2014). Previous studies showed that patient-derived fibroblasts harboring the pathogenic SPG3A (p.P342S) mutation could be reprogrammed and differentiated into forebrain neurons, enabling the identification of neurite outgrowth defects and reduced mitochondrial transport in mutant cells (Denton et al., 2014). Although this approach is promising, it remains to be determined whether the observed phenotypes are a direct result of the SPG3A (p.P342S) mutation alone or a combination of the hypomorphic SPG3A allele with other genetic variants in the background used. More recently, clustered regularly interspaced short palindromic repeats (CRISPR)-mediated genome editing has been used to correct mutations implicated in disease and determine their relevance to phenotypes observed (Xie et al., 2014; Li et al., 2015). Nevertheless, the use of patient-derived iPSCs introduces genetic variability, which can complicate the interpretation of data collected.

More than 70 genetic loci have been linked to the various forms of HSP, with most gene products identified possessing putative roles in axon pathfinding, axon myelination, organelle dynamics, motor-dependent transport, and/or lipid metabolism (Lo Giudice et al., 2014). In the majority of cases, there is minimal information regarding the functional consequences of the specific mutations identified. Here, we use a combination of structural biology, stem cell technology, and high-resolution imaging to define the impact of the TFG (p.R106C) mutation. Our findings demonstrate that the mutation impairs TFG complex assembly, which interferes with its function in the early secretory pathway, promotes ER

stress, and disrupts the ability of axons to selfassociate. These data suggest that the long axons of the corticospinal tract are particularly susceptible to relatively modest deficits in protein secretion and highlight this pathway as a potential therapeutic target for axonopathies that affect peripheral motor function.

RESULTS

A Clinically Relevant Mutation in TFG Disrupts Its Ability to Form Compact Ring Complexes

Mutations within the TFG coiled-coil domain (amino acids 97–124) have been suggested to impair its function and underlie early-onset forms of HSP (Beetz et al., 2013; Harlalka et al., 2016). To gain an understanding of the mechanism by which such mutations affect TFG, we conducted a series of biochemical and structural studies comparing the recombinant wildtype protein with the TFG (p.R106C) mutant, which has been identified in numerous HSP patients. Since the C terminus of TFG is intrinsically disordered (Johnson et al., 2015), we focused our attention on the TFG N terminus (amino acids 1–193), which includes a PB1 domain (amino acids 10–91), as well as the coiled-coil domain, followed by a serine/threonine-rich region (Figure 1A). We showed previously that the TFG (p.R106C) mutation modestly alters the hydrodynamic properties of TFG (Beetz et al., 2013), but its specific impact on the helical character of the coiled-coil domain remains unclear. To address this issue, we first conducted circular dichroism (CD) spectroscopy on various TFG isoforms. These studies revealed no significant differences in the helicity of the TFG (p.R106C) mutant as compared to wildtype TFG (Figure 1B). In contrast, mutation of six key leucine residues to valine (L97V, L105V, L109V, L112V, L120V, and L123V), which is predicted to completely disorder the heptad repeat pattern of the coiled-coil domain, resulted in a dramatic change in the circular dichroism spectrum, consistent with a loss in overall helicity (Figure 1B). We next examined the hydrodynamic properties of the isolated coiled-coil domain of wild-type TFG and the TFG (p.R106C) mutant. Based on a combination of size exclusion chromatography and multiangle light scattering, both proteins exhibited a similar ability to homo-oligomerize *in vitro* (Figures 1C and1D). In contrast, mutation of the six leucine residues within the coiled-coil domain to valine blocked self-association, resulting in the presence of monodisperse monomers of approximately 26 ± 3 kDa in mass (predicted molecular weight of 20.1 kDa) (Figures 1C and1D). Together, these data indicate that the TFG (p.R106C) mutation does not fully disrupt or unfold the coiled-coil domain.

To gain further insight into the impact of the TFG (p.R106C) mutation, we next used small-angle X-ray scattering (SAXS), a solution-based technique that can report on the conformation of biological macromolecules (Putnam et al., 2007). We used a smaller fragment of TFG for these studies (amino acids 1–138) to facilitate ab initio modeling. SAXS analysis of wild-type TFG produced consistent scattering profiles over several protein concentrations (150–750 mM) (Figure 1E), and the excluded particle (Porod) volume was used to estimate its mass to be 130 kDa, consistent with the predicted mass of 126.1 kDa for a TFG octamer, based on amino acid composition. From these data, we also determined the radius of gyration (R_g) to range from 35.1 ± 0.1 Å (750 mM) to 38.0 ± 0.3 Å(150 mM), depending on protein concentration (Figures S1A–S1C). Similarly, the maximal inter-atomic

distance (D_{max}) was concentration dependent, ranging from 94 to 120 Å , with higher compaction of the octamer observed at elevated protein concentrations (Figure S1C). SAXS envelopes were defined ab initio based on the scattering profiles. Seventeen independent models were aligned and averaged (based on two different protein concentrations), with a mean normalized spatial discrepancy (NSD) of 0.83, to reveal an octameric ring-like structure comparable in organization to that defined previously by three-dimensional single-particle electron microscopy (Figure 1F). The extensive similarity of the envelope with our prior electron microscopy-based analysis of TFG validates the use of SAXS for studying the impact of the TFG (p.R106C) mutation on the conformation of the octameric complex (Figure S1D).

SAXS analysis of TFG (p.R106C) produced consistent scattering profiles over the same protein concentrations examined for the wild-type protein (150–750 mM) (Figure 1G). However, in contrast to the wild-type protein, TFG (p.R106C) exhibited significantly higher R_g values (41.5 ± 0.9 Å , 150 mM; 41.3 ± 1.2 Å, 375 mM; 41.6 ± 1.0 Å , 750 mM) that did not vary based on protein concentration (Figures S1E and S1F). The D_{max} of TFG (p.R106C) was similarly concentration independent (on average, 141 ± 4 Å), suggesting a less compact organization relative to the wildtype protein (Figure S1C). Based on the scattering profiles collected at two protein concentrations, SAXS envelopes were defined ab initio. Twenty independent models were aligned and averaged, with a mean NSD of 0.90, to reveal a larger, more asymmetric assembly, as compared to the wild-type protein complex (Figure 1H). Collectively, these data suggest that the TFG (p.R106C) mutation impairs the function of the coiled-coil domain to generate compact octameric ring-like complexes.

To investigate this idea further, we examined the conformation of the TFG N terminus lacking the entire coiled-coil domain (amino acids 1–96) using SAXS. Based on hydrodynamic studies and multiangle light scattering, this region of TFG formed oligomers in solution (Figure S1G), consistent with the presence of a type I/II PB1 domain (Sumimoto et al., 2007). SAXS analysis of this TFG fragment produced consistent scattering profiles irrespective of protein concentration (450–900 mM), and we determined the radius of gyration (R_g) to be 36.1 ± 0.2 Å, with a D_{max} of 105 Å (Figures S1H and S1I). Twenty independent models were aligned and averaged (based on two different protein concentrations), with a mean NSD of 0.90, to reveal an oligomer in the shape of a curved tube (Figure S1J). This conformation closely resembles that of the intact TFG N terminus harboring its coiled-coil domain, except that key contacts necessary to bring together the ring-like structure appear to be absent. These data support the idea that the coiled-coil domain plays an important role in regulating TFG complex assembly to generate compact ring structures.

To directly visualize differences in the wild-type and mutant TFG complexes, we used single-particle electron microscopy. As described previously (Johnson et al., 2015), wild-type TFG typically forms ring-like structures that are approximately 10–11 nm in diameter, as visualized under negative stain (Figure 2A). In contrast, under identical buffer conditions (50 mM HEPES, pH 7.6; 100 mM NaCl), TFG (p.R106C) complexes exhibited a more heterogeneous arrangement of protomers and largely failed to form compact ring structures (Figure 2B). Notably, the predicted isoelectric point for TFG is 5.5. We therefore dialyzed

the wild-type TFG complexes into a buffer with this pH and observed that they exhibited reduced aggregation and improved staining homogeneity. Under these conditions, the propensity of TFG (p.R106C) complexes to form ring structures was increased (Figure 2C), consistent with the idea that the mutant protein is deficient for normal assembly but that the equilibrium can be shifted by lowering the pH. Nevertheless, although the TFG (p.R106C) mutant appeared capable of forming ring-like structures under these buffer conditions, we found that individual particles appeared more disorganized and distorted as compared to the wild-type protein (Figure 2D). In contrast, mutation of six leucine residues to valine within the coiled-coil domain blocked TFG ring assembly (Figure S2A). Collectively, our findings strongly suggest that the TFG (p.R106C) mutation specifically perturbs the normal conformation of TFG ring structures without having a dramatic effect on the ability of TFG protomers to self-associate.

To determine whether the specific presence of a positively charged residue at amino acid 106 in TFG is important for normal ring assembly, we additionally examined a TFG (p.R106K) mutant. We found that this mutation neither impaired the ability of the coiled-coil domain to self-associate, nor did it perturb the overall architecture of TFG ring complexes, even at neutral pH (Figures S2B and S2C). However, the clinically relevant TFG (p.R22W) mutation, which is located within the PB1 domain and also underlies an early-onset form of complicated HSP (El-sayed et al., 2016), caused a similar perturbation in ring assembly as compared to the TFG (p.R106C) mutation (Figure S2D), suggesting that proper folding and self-association of the PB1 domain is also critical for TFG complex formation. Consistent with this idea, examination a TFG (p.K14A) mutant, which impairs the ability of type I/II PB1 domains to self-associate (Sumimoto et al., 2007), strongly inhibited TFG ring assembly under all conditions tested (Figure S2E). Together, these data underscore the importance of both the PB1 and coiled-coil domains in assembling TFG complexes with a functional conformation.

To determine whether the altered conformation of TFG (p.R106C) affects its distribution in cells, we initially used a replacement strategy in which endogenous TFG is depleted using an siRNA targeting its 3′-UTR and an exogenous, doxycycline inducible isoform is expressed after directed transgene insertion into the “safe harbor” AAVS1 locus (Johnson et al., 2015; Qian et al., 2014). Using this system, we found that wildtype TFG accumulates with markers of COPII transport at the ER/ERGIC interface in human hTERT-immortalized RPE-1 cells (Figures S2F and S2G). Similarly, a mutation in the coiled-coil domain that maintains positive charge at residue 106, TFG (p.R106K), failed to perturb its distribution in cells (Figures S2F and S2G). In contrast, at similar levels of expression (Figure S2H), TFG (p.R106C) exhibited reduced accumulation at the ER/ ERGIC interface, as did another mutant that neutralizes positive charge at residue 106, TFG (p.R106A) (Figures S2G and S2I). Additionally, the TFG (p.R106C and p.R106A) mutations led to the appearance of more TFG-positive structures that failed to exhibit staining for COPII components, including several enlarged foci that exhibited high levels of the mutant TFG proteins (Figures S2I and S2J) Mutation of six leucine residuces to valine within the coiled-coil domain resulted in a dramatic redistribution of TFG away from the ER/ERGIC interface, further highlighting the importance of this domain to proper TFG localization (Figure S2K).

The TFG (p.R106C) Mutation Impairs Secretory Protein Trafficking and Elevates ER Stress

To establish a more physiologically relevant system to define the impacts of the TFG (p.R106C) mutation, we leveraged CRISPR technology to incorporate two nucleotide changes into well-characterized IMR90–4 human iPSCs. The first edit (c.316C>T) corresponds to the mutation found in HSP patients, while the second (c.321A>C) is silent, but introduces a novel restriction site to facilitate the identification of genome-edited cells. We screened a total of 300 edited clonal cell lines by PCR and restriction digest after single-cell sorting and identified 25 candidates for direct sequencing. Of these, we selected three homozygous clones (clones A–C), three heterozygous clones (clones D–F), and a control clone that was homozygous for the c.321A>C silent mutation, but failed to incorporate a change at nucleotide 316 (clone G) for further analysis (Figure 3A). Upon passaging, each clone exhibited a similar morphology as compared to IMR90–4, growing as individual colonies, and all stained positively for pluripotency markers, including Nanog, SSEA4, and Oct4 (Figures 3B and S3A). Additionally, karyotype analysis revealed no discernable defects in any of the clones following CRISPRmediated genome editing (Figures 3C and S3B).

We and others have shown previously that TFG is expressed ubiquitously in mammals (Beetz et al., 2013; Maebayashi et al., 2012). To determine the impact of the TFG (p.R106C) mutation, we differentiated each human iPSC clone toward a variety of cell fates. Given the importance of TFG at the ER/ERGIC interface, we initially generated tyrosinase-positive melanocytes (ectodermal lineage) and vimentin-positive fibroblasts (mesodermal lineage), both of which are amenable to assays for secretory pathway function (Figure S4A). Based on immunoblot analysis, TFG expression levels were not affected by presence of the p.R106C mutation in either cell type (Figures S4B and S4C). Immunofluorescence staining revealed that TFG (p.R106C) expressed at endogenous levels accumulated normally at the ER/ERGIC interface in homozygous, genome-edited fibroblast clones (Figures 4A, 4B, and S4D). However, in differentiated melanocytes, TFG (p.R106C) exhibited diminished co-localization with COPII transport carriers, relative to wild-type TFG (Figures 4C and4D). Instead, we consistently observed numerous structures, which labeled positively for TFG, but lacked other components of the early secretory pathway. Moreover, we found that the levels of TFG (p.R106C) at the ER/ERGIC interface were modestly, but significantly reduced as compared to wild-type TFG in control melanocytes (Figure S4D). Based on two-hybrid analysis, this was not due to a defect in the ability of TFG to associate with the COPII component Sec23 (Figure S4E), which we showed previously to be critical for TFG accumulation at the ER/ERGIC interface (Hanna et al., 2017). Together, these data indicate that the TFG (p.R106C) mutation affects its distribution, but only in a cell-type-specific manner.

To define potential impacts on early secretory pathway function, we transduced iPSC-derived melanocytes with a retrovirus encoding a GFP-tagged, temperature-sensitive form of vesicular stomatitis virus G protein (VSVG) (ts045), which misfolds and accumulates in the ER at 40oC, but folds properly and is capable of ER exit upon shift to 32oC (Presley et al., 1997). Cells expressing low levels of VSVG were imaged live following temperature shift. In control melanocytes, VSVG moved rapidly from the ER and began to accumulate in the perinuclear Golgi within 5–7 min (Figure 5A). Although the average timing of VSVG

appearance at the Golgi did not differ significantly in melanocytes expressing TFG (p.R106C), we observed prolonged accumulation of the cargo at punctate structures throughout the peripheral ER in mutant cells relative to controls, suggesting a delay during transport through the early secretory pathway (Figures 5A and5B). Specifically, in contrast to control melanocytes, which exhibited only transient elevations in VSVG intensity at punctate structures prior to Golgi accumulation, VSVG levels accumulated to higher levels at such sites and persisted for a longer period of time in melanocytes expressing TFG (p.R106C) (Figures 5A and5B).

Defects in the kinetics of protein secretion are often associated with an elevated unfolded protein response (UPR) (Wu and Kaufman, 2006). To determine whether the TFG (p.R106C) mutation leads to an activation of ER stress sensors, we stably transduced iPSC-derived fibroblasts and melanocytes to express a luciferase-based reporter of XBP1 mRNA splicing (Jheng et al., 2010). Control iPSC-derived cells exhibited negligible levels of luciferase luminescence, but treatment with a low concentration of tunicamycin, which leads to protein misfolding in the ER, resulted in an increase in XBP1 mRNA splicing (Figure S4F). Melanocytes exhibited a particularly strong ER stress response, as compared to fibroblasts. Strikingly, even in the absence of tunicamycin, cells expressing the homozygous TFG (p.R106C) mutation also exhibited elevated XBP1 mRNA splicing (Figure S4F), consistent with our finding that these cells show a kinetic delay in protein secretion from the ER. Since XBP1 mRNA splicing is largely regulated by the IRE1 ER stress sensor, we directly examined its activity in control and TFG (p.R106C) melanocytes by assessing the phosphorylation state of its kinase activation loop (Prischi et al., 2014). Immunoblot analysis confirmed that cells expressing the homozygous TFG (p.R106C) mutation exhibit constitutive activation of the IRE1 branch of the UPR (Figure 5C).

To determine whether heightened IRE1 activity sensitizes TFG (p.R106C)-expressing cells to additional forms of ER stress, we examined cargo transport to the Golgi following treatment and washout of brefeldin A (BFA), a fungal metabolite that inhibits guanine nucleotide exchange activity on several Arf-type GTPases, leads to the redistribution of integral membrane Golgi proteins to the ER, and dramatically increases ER stress signaling (Helms and Rothman, 1992; Citterio et al., 2008). For this assay, we transfected iPSC-derived fibroblasts and melanocytes with a GFP fusion to the transmembrane Golgi enzyme mannosidase II (ManII). In the absence of BFA, ManII accumulated at the Golgi in all clones, irrespective of the TFG isoform expressed, and addition of BFA resulted in the expected redistribution of ManII to the ER (Figure 5D). Within 120 min after BFA removal, more than 80% of control fibroblasts exhibited complete re-accumulation of ManII at the Golgi (Figures 5D and5E). In contrast, fibroblasts that were homozygous for the TFG (p.R106C) mutation largely retained ManII in the ER at this time point (Figures 5D and5E). After an extended period of washout, ManII was ultimately able to reach the Golgi in the mutant fibroblasts, again indicating that the TFG (p.R106C) mutation impairs the kinetics of protein secretion but does not block it (Figure 5D). Similarly, melanocytes harboring the homozygous TFG (p.R106C) mutation also exhibited a delay in ManII trafficking to the Golgi following BFA washout (Figure 5F). Together, our findings suggest that hypomorphic mutations in TFG, which disrupt its ring-like conformation, impact protein trafficking and the ER stress response in multiple cell lineages.

The Distribution of TFG in Cortical Neurons Is Disrupted by the p.R106C Mutation

Patients with the TFG (p.R106C) mutation exhibit progressive loss of gait and motor control, suggesting a particularly important function for TFG in neurons of the corticospinal tract (Beetz et al., 2013). We therefore used control and genome-edited iPSCs to generate Tbr1- and Tau-positive glutamatergic cortical neurons using established protocols (Figures S5A and S5B). The timing of differentiation was indistinguishable between control and TFG (p.R106C) mutant cells (Figure S5C), and similar to iPSC-derived fibroblasts and melanocytes, the overall levels of TFG in differentiated cortical neurons were not affected by the presence of the p.R106C mutation (Figure S5D). qPCR analysis further indicated that expression of TFG was also unaffected by presence of the mutation (Figure S5E). Additionally, wholecell patch-clamp recordings revealed no significant differences in synaptic activity or the membrane properties of homozygous TFG (p.R106C) neurons as compared to control (Figures S6A–S6C). These studies suggest that the TFG (p.R106C) mutation does not inhibit the differentiation of cortical neurons nor their spontaneous electrical activity *in vitro*.

We next examined early secretory pathway organization in iPSC-derived neurons, focusing on the distribution of markers associated with the Golgi apparatus and formation of COPIIcoated transport carriers. Using antibodies directed against GM130, a cis-Golgi matrix tethering protein, we found that the Golgi was largely limited to cell bodies in control neurons, juxtaposed to the nucleus, and homozygous expression of TFG (p.R106C) failed to dramatically impact its distribution or morphology (Figure S6D). In contrast, the localization of TFG in the mutant neurons was perturbed, similar to what we observed in iPSC-derived melanocytes. Specifically, we found that TFG (p.R106C) was more poorly retained at the ER/ERGIC interface in cell bodies and exhibited a more diffuse distribution throughout neurons (Figures 6A and S6D). These data are consistent with the idea that the p.R106C mutation alters TFG localization, most prominently in cells of the ectodermal lineage. Based on a previous study, overexpression of TFG (p.R106C) in primary murine hippocampal neurons results in the fragmentation of mitochondria (Harlalka et al., 2016). The mechanistic basis of this effect is unknown. However, our findings in RPE-1 cells indicate that overexpressed TFG (p.R106C) exhibits an enhanced propensity to form enlarged aggregates (see Figure S2I), which contrasts the distribution of the mutant protein when expressed at endogenous levels, and may indirectly affect mitochondrial morphology. We therefore conducted measurements of mitochondrial volume in Tau-positive neurites following differentiation of genome-edited human iPSCs. Our analysis revealed no significant discrepancies between the control and TFG (p.R106C) mutant neurons (Figure S6E). We additionally analyzed mitochondrial motility and found no significant differences in the percentage of motile mitochondria, nor their average rate of movement in neurites (Figure S6F). Together, these data suggest that that presence of the TFG (p.R106C) mutation is unlikely to have a direct effect on mitochondrial dynamics, including fission/fusion events.

Recent studies have also suggested that lysosomal defects are commonly associated with several mutations underlying HSPs (Allison et al., 2017). We therefore immunostained control and TFG (p.R106C) mutant neurons with the late endosome/ lysosome marker LAMP-1 and measured the volumes of structures identified in cell bodies. Our analysis

failed to demonstrate any differences in lysosome size or morphology between control and TFG (p.R106C) mutant neurons (Figure S6G), and we also failed to observe lysosome-enriched axonal swellings, as previously observed in mutant SPG4 patient-derived neurons (Denton et al., 2014; Allison et al., 2017). Similarly, changes in autophagic flux, which have been frequently associated with neurodegenerative diseases (Menzies et al., 2017), were not detected in TFG (p.R106C) mutant neurons, as indicated by the relative levels of lipidated (LC3-II) versus non-lipidated (LC3-I) LC3 (Figure S6H).

TFG Functions to Promote Axon Bundling

Previous work suggested that defects in ER structure/function caused by mutations in SPG3A (atlastin-1) contribute to neurodegenerative disease by impairing axon growth (Denton et al., 2014). To determine whether the TFG (p.R106C) mutation causes a similar effect, we generated iPSC-derived neurospheres and measured axon outgrowth following their transfer to coverslips. We found that homozygous neurons expressing TFG (p.R106C) extended axons to a similar length as observed in control neurons (Figures 6B and6C). However, during these studies, we also noted that control axons rapidly form bundles after emerging from neurospheres (Figure 6B). In contrast, neurons expressing TFG (p.R106C) failed to exhibit normal axon fasciculation (Figures 6B and6D). We also examined iPSC-derived neurons expressing the dominant-acting SPG3A (p.P342S) mutation and found that axon bundling occurred normally (Figure 6D). Together, these data suggest that TFG plays a distinct role from other regulators of ER function in axon maintenance.

Since our earlier studies suggested that the TFG (p.R106C) mutation causes an elevation in ER stress, we investigated the possibility that increased UPR signaling may affect the ability of axons to bundle. In an attempt to test this idea, we treated neurospheres with a low concentration of tunicamycin that was sufficient to activate IRE1, and examined neurite morphology over several days. Within 2 days of treatment, neurite outgrowth was found to be significantly impaired, and by day 5, neurites had largely undergone retraction and degeneration (Figure S7), preventing us from determining whether axon bundling was directly impacted. We therefore decided to explore alternative mechanisms by which the TFG (p.R106C) mutation might affect establishment or maintenance of axon contact.

Homotypic axon fasciculation is largely mediated by adhesion molecules that must be secreted to the surface of axonstoengage one another via extracellular domains (Winther and Walmod, 2014). Based on our findings that cells only expressing TFG (p.R106C)exhibitdefectsincargotransportfromtheER,wespeculated that the defect in axon bundling may result from impaired trafficking of adhesion molecules. To address this possibility, we stained genome-edited iPSC-derived neurons using antibodies directed against a subset of calcium-dependent and calciumindependent cell adhesion molecules (Sheng et al., 2013). As compared to controls, we found that the levels of cell surface L1CAM in particular were reduced in the axons of neurons expressing TFG (p.R106C), consistent with the idea that its transport to the cell surface was impaired (Figures 7A and7B). Importantly, this change was not a result of diminished L1CAM expression (Figure 7C). Instead, these data suggest that efficient membrane trafficking in the early secretory

pathway plays a critical role in maintaining neuronal homeostasis, especially in the long corticospinal motor neurons that undergo degeneration in HSPs.

DISCUSSION

Over the past several years, it has become evident that ER homeostasis plays a critical role in maintaining neuronal health. Mutations in numerous factors that regulate ER structure and function have been linked to a variety of neurodegenerative diseases, potentially by affecting calcium signaling, lipid biosynthesis, membrane trafficking, and/or interorganellar communication (Blackstone, 2012; Fowler et al., 2016). Based on our previous work demonstrating that TFG regulates protein transport at the ER/ERGIC interface (Witte et al., 2011; Johnson et al., 2015; Hanna et al., 2017), we hypothesized that TFG variants implicated in neurological disorders impair the secretion of biosynthetic cargoes. Here, we find that iPSC-derived cortical neurons homozygous for TFG (p.R106C) exhibit reduced levels of an important adhesion molecule at the surface of axons, which impedes their ability to self-associate. Based on post-mortem studies, loss of axon fasciculation within the corticospinal tract is commonly associated with motor neuropathies (Robberecht and Philips, 2013). This defect may contribute to reduced nerve conduction speed, which has been documented in several HSP patients harboring mutations in the TFG N terminus (Beetz et al., 2013). Together, our findings highlight the importance of efficient secretory egress from the ER in maintaining proper neuronal function, especially in the long cortical neurons that extend into the spinal cord.

Our structural and biochemical studies indicate that pathological mutations in the TFG N terminus lead to conformational abnormalities in TFG complexes, which significantly affect their distribution, but only in certain cell types. Nonetheless, kinetic delays in protein secretion appear to be more widespread in cells expressing homozygous TFG (p.R106C). These findings suggest that the mutation in the TFG coiled-coil domain has at least two distinct effects, one of which is dependent on cell lineage, while the other is not. The distribution of a protein is often regulated by interacting partners, which may be differentially expressed in various tissues. For example, the membrane-associated protein CIP4 functions in the endocytic pathway in fibroblasts but regulates membrane protrusion in neurons and cancer cells, largely due to unique interactions in these different cell types (Saengsawang et al., 2012). Similarly, cortical neurons may express specific factors that facilitate TFG localization but are only able to function appropriately when TFG complexes adopt their compact ring-like architecture. Based on this idea, it follows that homozygous TFG (p.R106C) individuals exhibit pronounced CNS phenotypes, but more limited perturbations in other tissues.

Independent of cell type, homozygous expression of TFG (p.R106C) slows protein export from the ER, which likely underlies the constitutive elevation in ER stress we observe in both iPSC-derived fibroblasts and melanocytes. At a mechanistic level, it remains unknown how the TFG (p.R106C) mutation causes this defect. One possibility is that the conformational change in TFG ring complexes impairs their ability to concentrate at the ER/ERGIC interface to promote outer COPII coat dissociation, which is a prerequisite for ER-derived transport carriers to tether and fuse with ERGIC membranes (Hanna et al., 2017).

Alternatively, the loosely assembled TFG (p.R106C) oligomers may not function optimally to organize COPII budding sites, which could preferentially affect the transport of bulky, high-molecular-weight cargoes (McCaughey et al., 2016). The retention of such cargoes could subsequently lead to additional consequences, including an elevation of ER stress (Ríos-Barrera et al., 2017). Importantly, elevated ER stress resulting from a deficit in protein secretion may also contribute to neurodegeneration (Scheper and Hoozemans, 2015). Several studies have shown that neuronal ER stress is a hallmark of Alzheimer's disease, Huntington's disease, synucleinopathies, ALS, and prion disease, although many of the models used are based on the overexpression of mutated genes identified in patient studies (Valenzuela et al., 2016; Ogen-Shtern et al., 2016; Colla et al., 2012). Our findings here emphasize the danger of this approach, as ectopically overexpressed TFG (p.R106C) behaves differently in cells when compared to the mutant expressed at endogenous levels. Nevertheless, therapeutic strategies to reduce ER stress and the UPR have been used on several models of neurodegenerative disease with varying levels of success (Remondelli and Renna, 2017). Our data suggest that some HSPs may also respond to this approach, although improved animal models will be necessary to formally test this possibility.

Although we identified L1CAM as one particular cargo in neurons that seems to rely heavily on TFG function for efficient secretion, it is likely that other secretory proteins are similarly affected. Notably, L1CAM was one of the first genes implicated in the pathogenesis of HSP and mutations affecting it result in the most common form of X-linked HSP, often associated with the absence of L1CAM cell surface expression and impaired axonal adhesion (Lo Giudice et al., 2014; Barry et al., 2010; Schäfer and Frotscher, 2012). Patients expressing mutant isoforms of L1CAM typically exhibit thinning of the corpus callosum with early-onset leg spasticity, consistent with phenotypes observed in patients with mutations in TFG (Beetz et al., 2013; Schrander-Stumpel et al., 1995; Jouet et al., 1994). Our data demonstrating a defect in axon fasciculation in iPSC-derived neurons expressing TFG (p.R106C) further support an intimate connection between TFG function and L1CAM cell surface expression. Considering the length of neurons in the corticospinal tract, even minor perturbations to L1CAM trafficking may affect bundling of distal axon segments, especially during neurite outgrowth. In contrast, a similarly modest reduction in ER export in a fibroblast or melanocyte would have a more limited impact on cell growth. Confirmation of this idea will require further studies in patients with TFG mutations or the development of an appropriate animal model.

EXPERIMENTAL PROCEDURES

Recombinant Protein Expression and Purification

All recombinant proteins were expressed using BL21(DE3)-T1R bacteria (Sigma-Aldrich) and purified initially using glutathione agarose beads (for GST-fusion proteins) or nickel affinity resin (polyhistidine-tagged proteins). Eluted or cleaved proteins were subsequently applied onto ion exchange and/or gel filtration columns for further purification (Johnson et al., 2015). For circular dichroism spectroscopy, purified proteins were analyzed using a 0.1-cm path length quartz cell in 25 mM sodium phosphate (pH 7.2). Spectra were collected using a model 202SF circular dichroism spectrophotometer at 25C. For mass determination,

proteins were examined by dynamic light scattering using a Wyatt mini-DAWN TREOS three-angle light-scattering detector coupled to a high-resolution size exclusion chromatography system. ASTRA software was used to calculate molecular mass (Schuh et al., 2015).

SAXS Data Collection

Data were collected at sector 12-ID-B of the Advanced Photon Source (APS) at Argonne National Laboratory and obtained at a wavelength of 1.54 Å and a sample-detector distance of 4 m (small-angle) and 30 cm (wide-angle) resulting in a total momentum transfer range of $0.01 < q < 2.31$ Å 1. Data were collected for buffer and protein at 25C for 2 min (APS), and buffer subtraction was adjusted for the excluded volume of the protein. The predicted scattering intensity at q = 0 Å 1 and the radius of gyration (R_g) were determined by Guinier analysis (Putnam et al., 2007) and compared between two to three concentrations to detect interparticle interference and concentration-dependent changes in conformation.

Single-Particle Electron Microscopy

Purified proteins (4 μL) at a concentration of 0.01 mg/mL were placed on plasma-cleaned carbon-coated grids, washed with water, and stained with 2% uranyl formate as described previously (Johnson et al., 2015). Imaging was conducted using an FEI Titan Krios transmission electron microscope operated at 120 keV and equipped with a Gatan Ultrascan 4,000 3 4,000 charge-coupled device (CCD) camera. Class averages were generated by reference-free alignment (Johnson et al., 2015).

CRISPR-Mediated Genome Editing

For CRISPR-mediated editing, iPSCs were electroporated with a plasmid encoding Cas9-GFP, a guide RNA targeting TFG (5'-GAAGTTCTATCAGTT CTCGA-3'), and a single-stranded oligonucleotide to incorporate the desired point mutations via homology directed repair. Cells were sorted using a BD FACSAria III cell sorter based on GFP fluorescence, and individual colonies were harvested after 1 week and moved to individual Matrigel-coated dishes. The incorporation of point mutations was confirmed following genomic DNA preparation, PCR amplification, and Sanger sequencing. For karyotype analysis, Giemsa banding was outsourced to WiCell Cytogenetics Laboratory. Stem cell maintenance and differentiation procedures are detailed in Supplemental Experimental Procedures.

Immunofluorescence and Confocal Microscopy

For immunofluorescence analysis, cells were fixed using paraformaldehyde (4%) and stained using primary antibodies at a final concentration of 1 μg/mL, as described previously (Johnson et al., 2015). Imaging was conducted on a swept-field confocal microscope using a Roper CoolSnap HQ2 CCD camera and a Nikon 603, 1.4 numerical aperture (NA) Plan Apo oil objective lens. Acquisition parameters were controlled by Nikon Elements, and image analysis was conducted using ImageJ or Imaris (Bitplane) software. BFA treatments (10 mg/mL) were each conducted for 1 hr at 37o C, followed by washout using pre-warmed media. Cells expressing GFP-tagged VSVG were incubated overnight at 40o C and subsequently placed into a Tokai Hit stage top incubator set to 32o C for live-cell imaging.

Particle tracking, volume measurements, and linescan analysis for intensity measurements were conducted in an unbiased manner using Imaris software.

Statistical Methods

All p values were determined by paired t test or ANOVA, calculated using Microsoft Excel or GraphPad Prism, and data are shown as mean ± SEM. Significant differences were indicated by a p value less than 0.05.

Supplementary Material

Refer to Web version on PubMed Central for supplementary material.

ACKNOWLEDGMENTS

This work was supported in part by NIH Grants GM110567 (to A.A.), GM086892 (to S.M.S.), HD076828 (to M.D.S.), and R35GM118131 (to S.E.B.); American Cancer Society Grant 123268-RSG-12–139-01-CSM (to A.A.); Brain Research Foundation Grant BRFSG-2015–03 (to A.A.); the Spastic Paraplegia Foundation; University of Wisconsin Carbone Cancer Center Grant P30 CA014520; and University of Wisconsin Institute for Clinical and Translational Research Grant UL1TR000427. This study made use of the National Magnetic Resonance Facility at Madison, which is supported by NIH Grant P41GM103399. SAXS studies were supported by funds from NIH Shared Instrumentation Grant S10RR027000 and the University of Wisconsin-Madison. Use of the Advanced Photon Source, an Office of Science User Facility operated for the U.S. Department of Energy (DOE) Office of Science by Argonne National Laboratory, was supported by the U.S. DOE under Contract No. DE-AC0206CH11357.

REFERENCES

Allison R, Edgar JR, Pearson G, Rizo T, Newton T, Günther S, Berner F, Hague J, Connell JW, Winkler J, et al. (2017). Defects in ER-endosome contacts impact lysosome function in hereditary spastic paraplegia. J. Cell Biol 216, 1337–1355. [PubMed: 28389476]

Barry J, Gu Y, and Gu C (2010). Polarized targeting of L1-CAM regulates axonal and dendritic bundling in vitro. Eur. J. Neurosci 32, 1618–1631. [PubMed: 20964729]

Beetz C, Johnson A, Schuh AL, Thakur S, Varga RE, Fothergill T, Hertel N, Bomba-Warczak E, Thiele H, Nürnberg G, et al. (2013). Inhibition of TFG function causes hereditary axon degeneration by impairing endoplasmic reticulum structure. Proc. Natl. Acad. Sci. USA 110, 5091–5096. [PubMed: 23479643]

Blackstone C (2012). Cellular pathways of hereditary spastic paraplegia. Annu. Rev. Neurosci 35, 25–47. [PubMed: 22540978]

Citterio C, Vichi A, Pacheco-Rodriguez G, Aponte AM, Moss J, and Vaughan M (2008). Unfolded protein response and cell death after depletion of brefeldin A-inhibited guanine nucleotide-exchange protein GBF1. Proc. Natl. Acad. Sci. USA 105, 2877–2882. [PubMed: 18287014]

Colla E, Coune P, Liu Y, Pletnikova O, Troncoso JC, Iwatsubo T, Schneider BL, and Lee MK (2012). Endoplasmic reticulum stress is important for the manifestations of α-synucleinopathy in vivo. J. Neurosci 32, 3306–3320. [PubMed: 22399753]

de Souza PVS, de Rezende Pinto WBV, de Rezende Batistella GN, Bortholin T, and Oliveira ASB (2017). Hereditary spastic paraplegia: clinical and genetic hallmarks. Cerebellum 16, 525–551. [PubMed: 27271711]

Denton KR, Lei L, Grenier J, Rodionov V, Blackstone C, and Li XJ (2014). Loss of spastin function results in disease-specific axonal defects in human pluripotent stem cell-based models of hereditary spastic paraplegia. Stem Cells 32, 414–423. [PubMed: 24123785]

Elsayed LE, Mohammed IN, Hamed AA, Elseed MA, Johnson A, Mairey M, Mohamed HE, Idris MN, Salih MA, El-Sadig SM, et al. (2016). Hereditary spastic paraplegias: identification of a novel SPG57 variant affecting TFG oligomerization and description of HSP subtypes in Sudan. Eur. J. Hum. Genet 25, 100–110. [PubMed: 27601211]

Fowler PC, Byrne DJ, and O'Sullivan NC (2016). Rare disease models provide insight into inherited forms of neurodegeneration. J. Rare Dis. Res. Treat 1, 17–21.

Hanna MG, 4th, Block S, Frankel EB, Hou F, Johnson A, Yuan L, Knight G, Moresco JJ, Yates JR, 3rd, Ashton R, et al. (2017). TFG facilitates outer coat disassembly on COPII transport carriers to promote tethering and fusion with ER-Golgi intermediate compartments. Proc. Natl. Acad. Sci. USA 114, E7707–E7716. [PubMed: 28851831]

Harlalka GV, McEntagart ME, Gupta N, Skrzypiec AE, Mucha MW, Chioza BA, Simpson MA, Sreekantan-Nair A, Pereira A, Günther S, et al. (2016). Novel genetic, clinical, and pathomechanistic insights into TFGassociated hereditary spastic paraplegia. Hum. Mutat. 37, 1157–1161. [PubMed: 27492651]

Helms JB, and Rothman JE (1992). Inhibition by brefeldin A of a Golgi membrane enzyme that catalyses exchange of guanine nucleotide bound to ARF. Nature 360, 352–354. [PubMed: 1448152]

Ishiura H, Sako W, Yoshida M, Kawarai T, Tanabe O, Goto J, Takahashi Y, Date H, Mitsui J, Ahsan B, et al. (2012). The TRK-fused gene is mutated in hereditary motor and sensory neuropathy with proximal dominant involvement. Am. J. Hum. Genet 91, 320–329. [PubMed: 22883144]

Jheng JR, Lau KS, Tang WF, Wu MS, and Horng JT (2010). Endoplasmic reticulum stress is induced and modulated by enterovirus 71. Cell. Microbiol 12, 796–813. [PubMed: 20070307]

Johnson A, Bhattacharya N, Hanna M, Pennington JG, Schuh AL, Wang L, Otegui MS, Stagg SM, and Audhya A (2015). TFG clusters COPII-coated transport carriers and promotes early secretory pathway organization. EMBO J. 34, 811–827. [PubMed: 25586378]

Jouet M, Rosenthal A, Armstrong G, MacFarlane J, Stevenson R, Paterson J, Metzenberg A, Ionasescu V, Temple K, and Kenwrick S (1994).X-linked spastic paraplegia (SPG1), MASA syndrome and X-linked hydrocephalus result from mutations in the L1 gene. Nat. Genet. 7, 402–407. [PubMed: 7920659]

Kawarai T, Morita M, Morigaki R, Fujita K, Nodera H, Izumi Y, Goto S, Nakano I, and Kaji R (2013). [Pathomechanisms of motor neuron death by mutant TFG]. Rinsho Shinkeigaku 23, 1199. [PubMed: 24291928]

Li HL, Fujimoto N, Sasakawa N, Shirai S, Ohkame T, Sakuma T, Tanaka M, Amano N, Watanabe A, Sakurai H, et al. (2015). Precise correction of the dystrophin gene in Duchenne muscular dystrophy patient induced pluripotent stem cells by TALEN and CRISPR-Cas9. Stem Cell Reports 4, 143–154. [PubMed: 25434822]

Lo Giudice T, Lombardi F, Santorelli FM, Kawarai T, and Orlacchio A (2014). Hereditary spastic paraplegia: clinical-genetic characteristics and evolving molecular mechanisms. Exp. Neurol. 261, 518–539. [PubMed: 24954637]

Maebayashi H, Takeuchi S, Masuda C, Makino S, Fukui K, Kimura H, and Tooyama I (2012). Expression and localization of TRK-fused gene products in the rat brain and retina. Acta Histochem. Cytochem. 45, 15–23. [PubMed: 22489101]

McCaughey J, Miller VJ, Stevenson NL, Brown AK, Budnik A, Heesom KJ, Alibhai D, and Stephens DJ (2016). TFG promotes organization of transitional ER and efficient collagen secretion. Cell Rep. 15, 1648–1659. [PubMed: 27184855]

Menzies FM, Fleming A, Caricasole A, Bento CF, Andrews SP, Ashkenazi A, Fu€llgrabe J, Jackson A, Jimenez Sanchez M, Karabiyik C, et al. (2017). Autophagy and neurodegeneration: pathogenic mechanisms and therapeutic opportunities. Neuron 93, 1015–1034. [PubMed: 28279350]

Ogen-Shtern N, Ben David T, and Lederkremer GZ (2016). Protein aggregation and ER stress. Brain Res. 1648 (Pt B), 658–666. [PubMed: 27037184]

Presley JF, Cole NB, Schroer TA, Hirschberg K, Zaal KJ, and Lippincott-Schwartz J (1997). ER-to-Golgi transport visualized in living cells. Nature 389, 81–85. [PubMed: 9288971]

Prischi F, Nowak PR, Carrara M, and Ali MM (2014). Phosphoregulation of Ire1 RNase splicing activity. Nat. Commun. 5, 3554. [PubMed: 24704861]

Putnam CD, Hammel M, Hura GL, and Tainer JA (2007). X-ray solution scattering (SAXS) combined with crystallography and computation: defining accurate macromolecular structures, conformations and assemblies in solution. Q. Rev. Biophys 40, 191–285. [PubMed: 18078545]

Qian K, Huang CT, Chen H, Blackbourn LW, 4th, Chen Y, Cao J, Yao L, Sauvey C, Du Z, and Zhang SC (2014). A simple and efficient system for regulating gene expression in human pluripotent stem cells and derivatives. Stem Cells 32, 1230–1238. [PubMed: 24497442]

Remondelli P, and Renna M (2017). The endoplasmic reticulum unfolded protein response in neurodegenerative disorders and its potential therapeutic significance. Front. Mol. Neurosci 10, 187. [PubMed: 28670265]

Ríos-Barrera LD, Sigurbjörnsdóttir S, Baer M, and Leptin M (2017). Dual function for Tango1 in secretion of bulky cargo and in ER-Golgi morphology. Proc. Natl. Acad. Sci. USA 114, E10389–E10398. [PubMed: 29138315]

Robberecht W, and Philips T (2013). The changing scene of amyotrophic lateral sclerosis. Nat. Rev. Neurosci 14, 248–264. [PubMed: 23463272]

Saengsawang W, Mitok K, Viesselmann C, Pietila L, Lumbard DC, Corey SJ, and Dent EW (2012). The F-BAR protein CIP4 inhibits neurite formation by producing lamellipodial protrusions. Curr. Biol. 22, 494–501. [PubMed: 22361215]

Saheki Y, and De Camilli P (2017). Endoplasmic reticulum-plasma membrane contact sites. Annu. Rev. Biochem. 86, 659–684. [PubMed: 28301744]

Scha¨ fer MK, and Frotscher M (2012). Role of L1CAM for axon sprouting and branching. Cell Tissue Res. 349, 39–48. [PubMed: 22370595]

Scheper W, and Hoozemans JJ (2015). The unfolded protein response in neurodegenerative diseases: a neuropathological perspective. Acta Neuropathol. 130, 315–331. [PubMed: 26210990]

Schrander-Stumpel C, Ho¨ weler C, Jones M, Sommer A, Stevens C, Tinschert S, Israel J, and Fryns JP (1995). Spectrum of X-linked hydrocephalus (HSAS), MASA syndrome, and complicated spastic paraplegia (SPG1): clinical review with six additional families. Am. J. Med. Genet 57, 107–116. [PubMed: 7645588]

Schuh AL, Hanna M, Quinney K, Wang L, Sarkeshik A, Yates JR, and Audhya A (2015). The VPS-20 Subunit of the Endosomal Sorting Complex ESCRT-III Exhibits an Open Conformation in the Absence of Upstream Activation. Biochem. J 466, 625–637. [PubMed: 25588614]

Sheng L, Leshchyns'ka I, and Sytnyk V (2013). Cell adhesion and intracellular calcium signaling in neurons. Cell Commun. Signal 11, 94. [PubMed: 24330678]

Sumimoto H, Kamakura S, and Ito T (2007). Structure and function of the PB1 domain, a protein interaction module conserved in animals, fungi, amoebas, and plants. Sci. STKE 2007, re6.

Valenzuela V, Martínez G, Duran-Aniotz C, and Hetz C (2016). Gene therapy to target ER stress in brain diseases. Brain Res. 1648 (Pt B), 561–570. [PubMed: 27131987]

Vazin T, Ball KA, Lu H, Park H, Ataeijannati Y, Head-Gordon T, Poo MM, and Schaffer DV (2014). Efficient derivation of cortical glutamatergic neurons from human pluripotent stem cells: a model system to study neurotoxicity in Alzheimer's disease. Neurobiol. Dis 62, 62–72. [PubMed: 24055772]

Wang X, Huang T, Bu G, and Xu H (2014). Dysregulation of protein trafficking in neurodegeneration. Mol. Neurodegener 9, 31. [PubMed: 25152012]

Weis J, Claeys KG, Roos A, Azzedine H, Katona I, Schro¨ der JM, and Senderek J (2017). Towards a functional pathology of hereditary neuropathies. Acta Neuropathol. 133, 493–515. [PubMed: 27896434]

Winther M, and Walmod PS (2014). Neural cell adhesion molecules belonging to the family of leucine-rich repeat proteins. Adv. Neurobiol 8, 315–395. [PubMed: 25300143]

Witte K, Schuh AL, Hegermann J, Sarkeshik A, Mayers JR, Schwarze K, Yates JR, 3rd, Eimer S, and Audhya A (2011). TFG-1 function in protein secretion and oncogenesis. Nat. Cell Biol 13, 550–558. [PubMed: 21478858]

Wu J, and Kaufman RJ (2006). From acute ER stress to physiological roles of the unfolded protein response. Cell Death Differ. 13, 374–384. [PubMed: 16397578]

Xie F, Ye L, Chang JC, Beyer AI, Wang J, Muench MO, and Kan YW (2014). Seamless gene correction of b-thalassemia mutations in patient-specific iPSCs using CRISPR/Cas9 and piggyBac. Genome Res. 24, 1526–1533. [PubMed: 25096406]

Yagi T, Ito D, and Suzuki N (2016). TFG-related neurologic disorders: new insights into relationships between endoplasmic reticulum and neurodegeneration. J. Neuropathol. Exp. Neurol 75, 299–305. [PubMed: 26945032]

Highlights

- Pathological mutations in TFG impair its ability to form compact ring complexes
- The TFG (p.R106C) mutation compromises the kinetics of secretory protein transport
- TFG promotes the accumulation of L1CAM at the surface of axons
- Partial inhibition of TFG function results in a defect in axon bundling

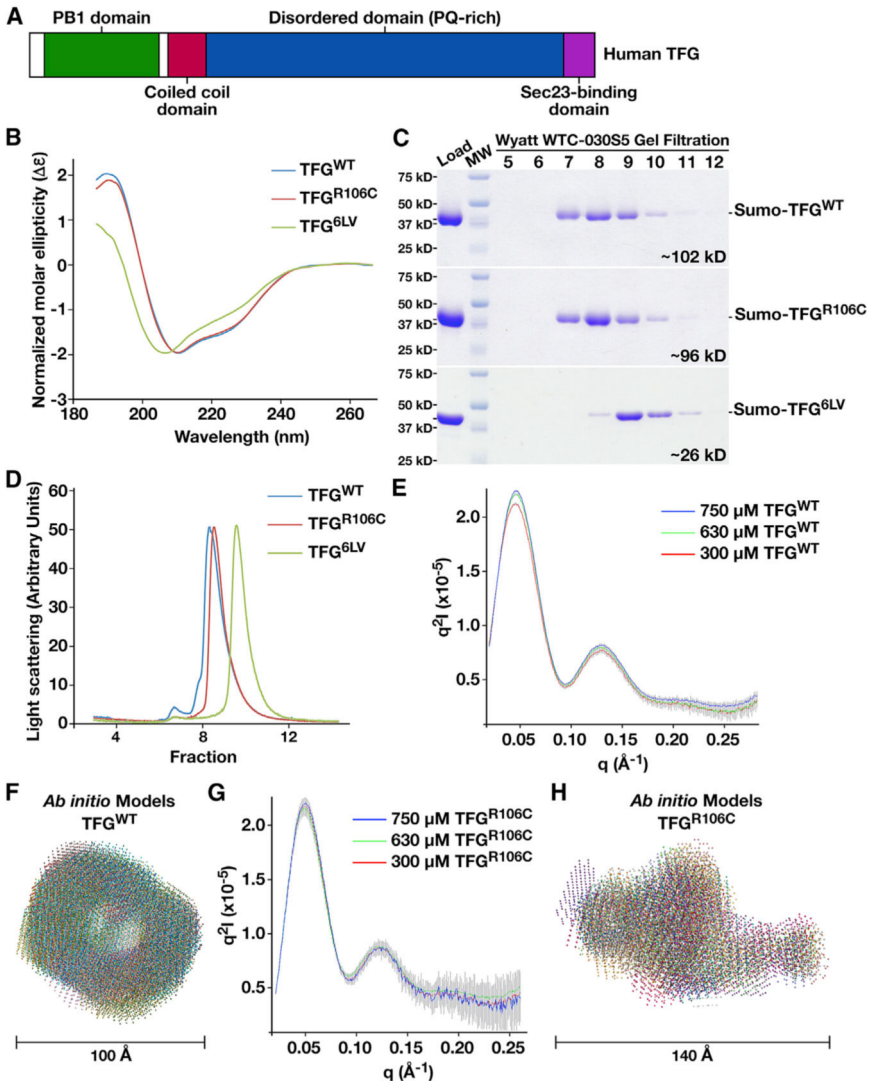

Figure 1. The TFG (p.R106C) Mutation Alters the Conformation of TFG Ring Complexes

(A)Cartoon highlighting the various domains of human TFG, including its PB1 domain (green), coiled-coil domain (red), disordered domain (blue), and Sec23-binding domain (purple).

(B) Circular dichroism (CD) spectroscopy was used to characterize the N terminus of various TFG isoforms (amino acids 1–193; wild-type TFG, TFG [p.R106C], and TFG harboring six leucineto-valine mutations throughout its coiled-coil domain; n = 3 for each).

(C and D) Purified recombinant isoforms of TFG (amino acids 92–138; wild-type TFG, TFG [p.R106C], and TFG harboring six leucine-tovaline mutations throughout its coiled-coil domain) fused to a monomeric SUMO tag were separated over a gel filtration column (Wyatt WTC-030S5) that was coupled to a multiangle light-scattering device. Eluted fractions were separated by SDS/ PAGE and stained using Coomassie Blue to highlight their elution profiles (C) (n = 3 each). Average molecular masses were calculated using ASTRA software (n = 3 each), and light-scattering profiles for each protein are shown (D).

(E and G) Representative Kratky scattering profiles generated from the analysis of three concentrations of wild-type TFG (E) or TFG (p.R106C) (G) following SAXS (n = 3 each). All experiments were conducted in 50 mM Tris-HCl, pH 7.6, 10 mM DTT, and 100 mM NaCl.

(F and H) Ab initio models of the N terminus (amino acids 1–138) of wild-type TFG (F) and TFG (p.R106C) (H). At least 17 structures of each protein were generated using the program DAMMIF, and dummy atom models were overlaid. The normalized spatial discrepancy (NSD) of the wild TFG SAXS envelope was 0.83, and the NSD of the TFG (p.R106C) mutant was 0.90.

See also Figure S1.

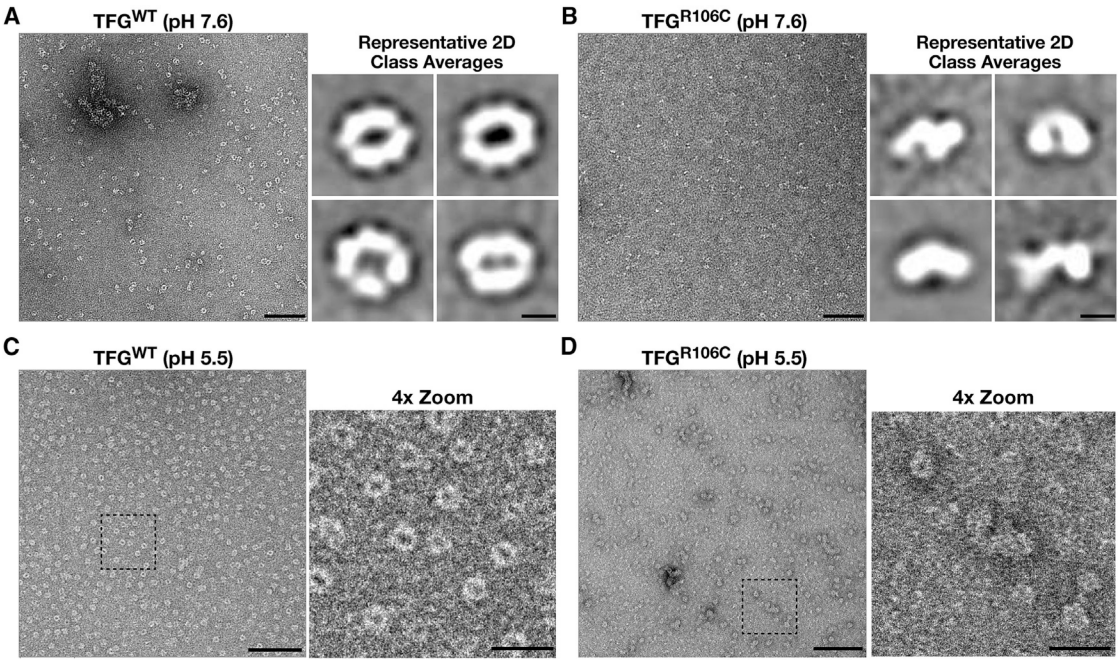

Figure 2. The TFG (p.R106C) Mutation Perturbs the Assembly of Compact Ring Structures

(A and B) Recombinant wild-type TFG (A) and TFG (p.R106C) (B) were imaged by negative-staining electron microscopy following purification in 50 mM HEPES, pH 7.6, and 100 mM NaCl (n = 3 each). Montage of representative class averages (amino acids 1–193 in both cases) generated by reference-free alignment and classification are shown (right panels). Scale bars, 100 nm (left) and 5 nm (right, class averages).

(C and D) Recombinant wild-type TFG (C) and TFG (p.R106C) (D) were imaged by negative-staining electron microscopy following purification in 50 mM MES, pH 5.5, and 100 mM NaCl (n = 3 each). Representative higher-magnification views of individual complexes are shown (right panels). Scale bars, 100 nm (left) and 25 nm (right).

See also Figure S2.

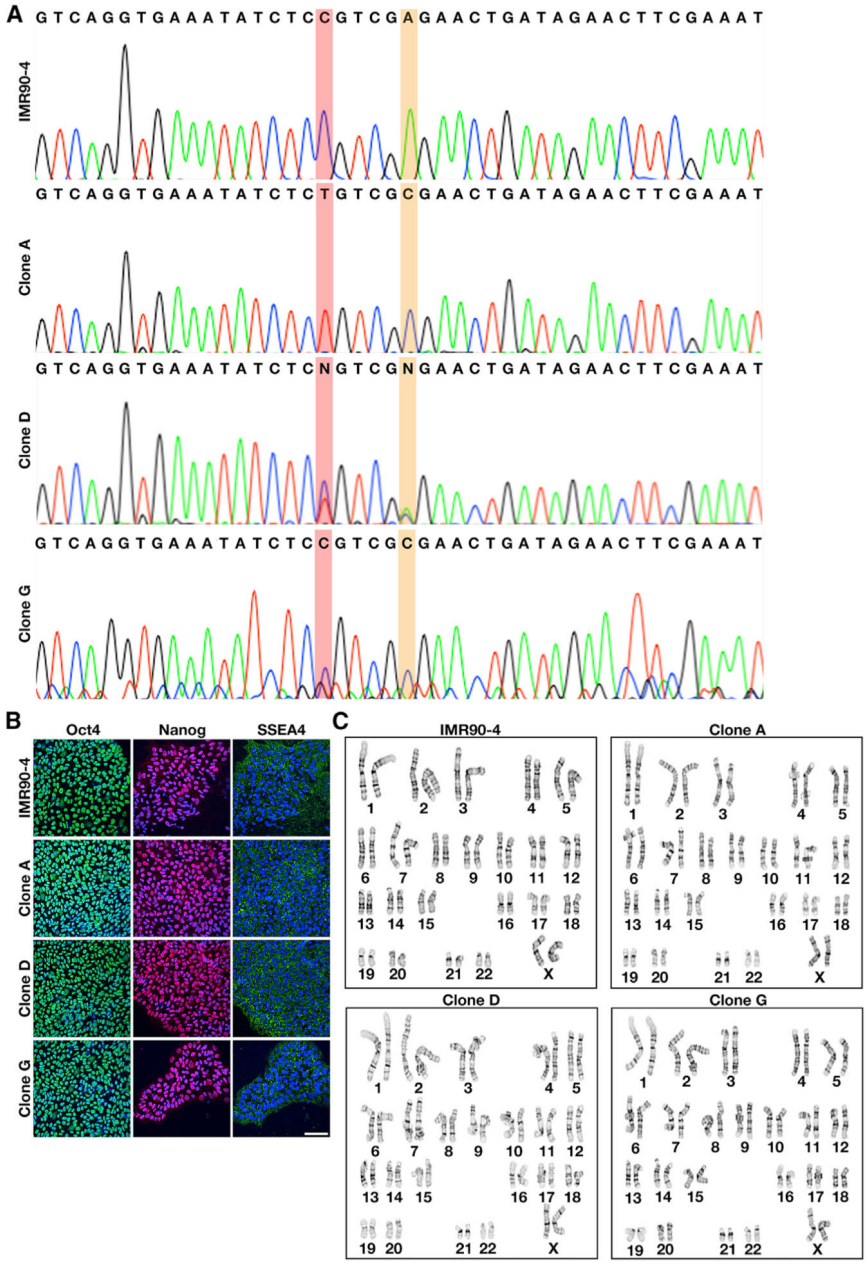

Figure 3. Generation of Human iPSCs Harboring the TFG (p.R106C) Mutation

(A)Representative Sanger sequencing traces ofTFG exon 4 from control (IMR90–4) and genome-edited (clones A, D, and G) iPSCs. The single-nucleotide change found in HSP patients is highlighted in red, while the silent mutation incorporated to enable facile identification of edited clones is highlighted in yellow.

(B) Control iPSCs (IMR90–4 and clone G) and iPSCs harboring a mutation in TFG (clones A and D) were fixed and stained using antibodies directed against Oct4, Nanog, and SSEA4 together with Hoechst 33342 (n = 3 each). Maximum intensity projections are shown. Scale bar, 100 mm.

(C) Giemsa banding analysis was performed oncontrol iPSCs (IMR90–4 and clone G) and iPSCs harboring a mutation in TFG (clones A and D), revealing no changes in karyotype that resulted from CRISPR-mediated genome editing.
See also Figure S3.

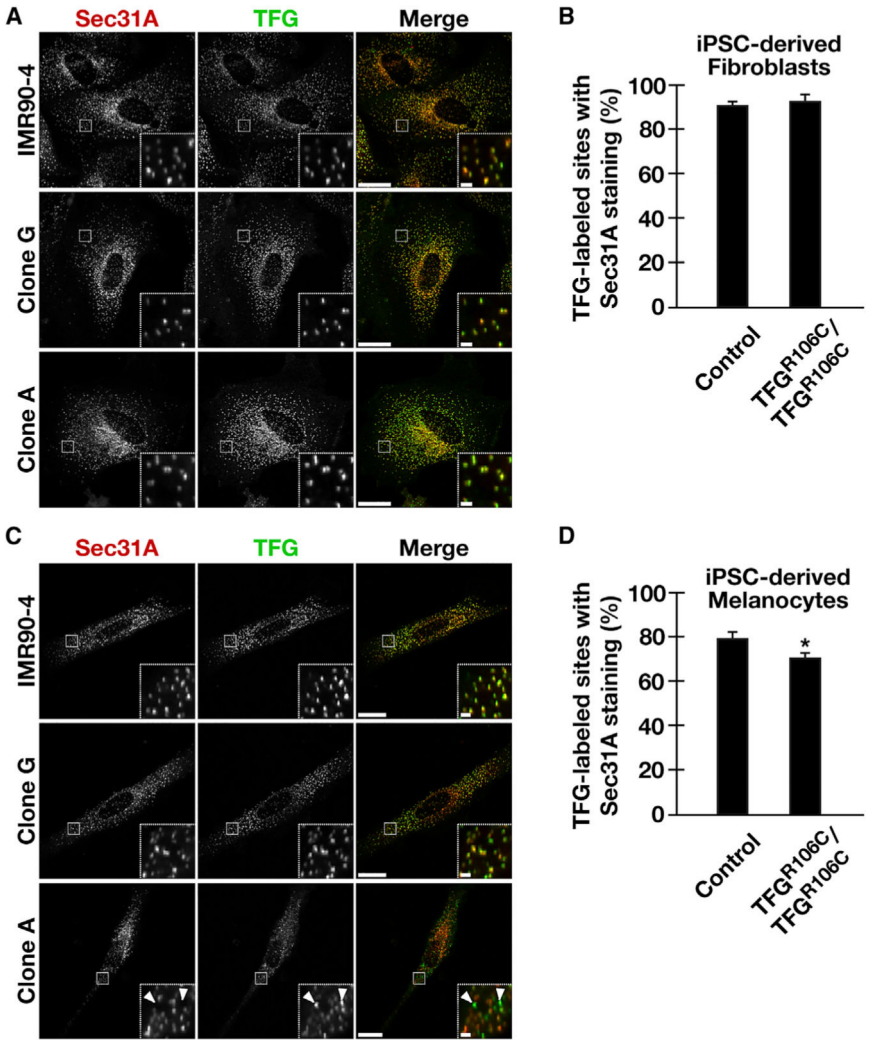

Figure 4. The TFG (p.R106C) Mutation Alters Its Distribution in a Cell-Type-Specific Manner

(A)Representative control (IMR90–4 and clone G) and homozygous TFG (p.R106C) expressing (clone A) iPSC-derived fibroblasts were fixed and stained using antibodies directed against Sec31A (red) and TFG (green) and imaged using sweptfield confocal optics. Maximum intensity projections are shown. Scale bars, 10 mm and 1 mm (insets).

(B) Quantification of the percentage of TFG-labeled structures that exhibit Sec31A staining in control (IMR90–4 and clone G) and homozygous TFG (p.R106C)-expressing fibroblasts (clones A, B, and C). Error bars represent mean ± SEM; n > 10 different cells per condition; three biological replicates each. No statistically significant difference was found, as calculated using a paired t test.

(C) Representative control (IMR90–4 and clone G) and homozygous TFG (p.R106C)-expressing (clone A) iPSC-derived melanocytes were fixed and stained using antibodies directed against Sec31A (red) and TFG (green) and imaged using swept-field confocal optics. Maximum intensity projections are shown. Scale bars, 10 mm and 1 mm (insets).

(D) Quantification of the percentage of TFGlabeled structures that exhibit Sec31A staining in control (IMR90–4 and clone G) and homozygous TFG (p.R106C)-expressing

melanocytes (clones A, B, and C). Error bars represent mean ± SEM; n > 10 different cells per condition; three biological replicates each. *p < 0.05, as calculated using a paired t test. See also Figure S4.

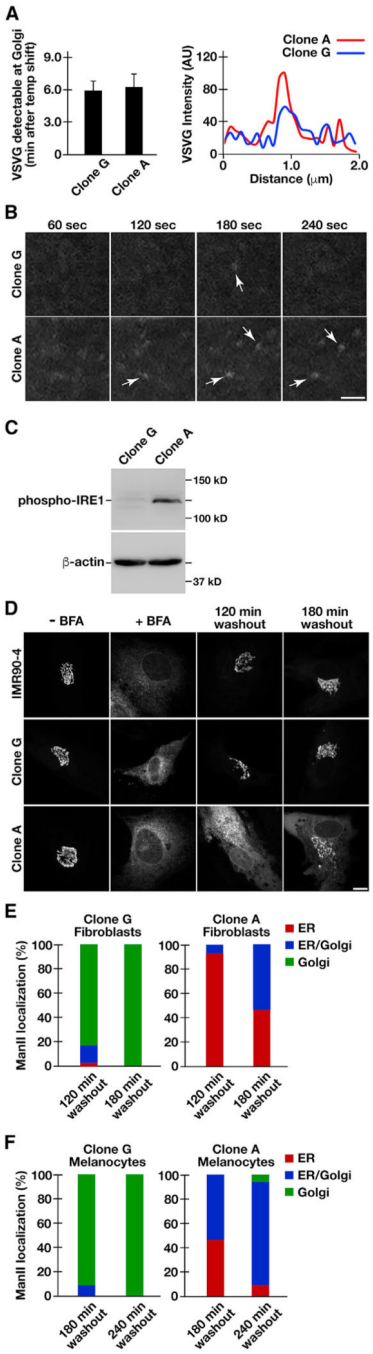

Figure 5. The TFG (p.R106C) Mutation Impairs Its Function in Differentiated Cells

(A) Representative control (clone G) and homozygous TFG (p.R106C)-expressing (clone A) iPSC-derived melanocytes were transduced to express ts045 VSVG-GFP and imaged live using swept-field confocal optics following shift to 32C. The period of time required for VSVG-GFP to reach the perinuclear Golgi, as determined by an elevation in fluorescence intensity relative to the surrounding ER, was measured in both cases (left). Error bars represent mean ± SEM; n > 5 different cells per condition. No statistically significant difference was found, as calculated using a paired t test. Representative linescan analyses

highlight the difference in the fluorescence intensity of VSVG-GFP that accumulates in punctate structures throughout the peripheral ER, prior to its appearance in the Golgi (right; n > 50 punctate structures per condition; five biological replicates each).

(B) Representative images of the peripheral ER obtained using swept-fieldconfocal optics in the iPSC-derived cell lines described in (A) at various time points after shift to 32C. Scale bar, 2 mm.

(C) Representative immunoblot analysis of extracts generated from control(clone G) and TFG (p.R106C) (clone A) iPSC-derived melanocytes using antibodies directed against phospho-IRE1 and b-actin (n = 3).

(D) Representative control (IMR90–4 and clone G) and homozygous TFG (p.R106C)-expressing (clone A) iPSC-derived fibroblasts transfected with ManII-GFP were incubated in the presence and absence of BFA or following BFA washout. Cells were fixed under the conditions indicated and imaged using swept-field confocal optics. Maximum intensity projections are shown.Scale bar, 10 mm.

(E and F) The distribution of ManII-GFP was quantified in control and TFG (p.R106C) iPSC-derived fibroblasts (E) and melanocytes (F) at two different time points following BFA washout. More than 100 cells were analyzed for each condition; three biological replicates each.

See also Figure S4.

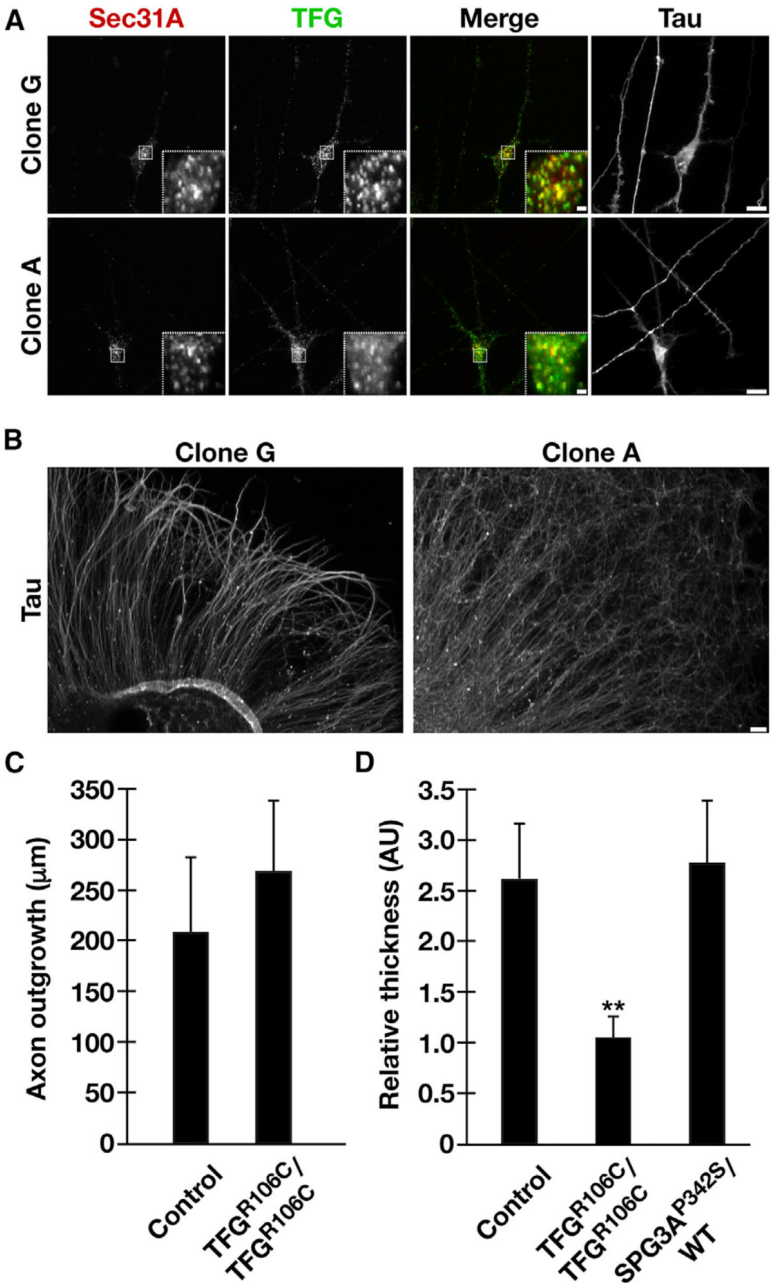

Figure 6. The TFG (p.R106C) Mutation Leads to a Defect in Axon Fasciculation in iPSC-Derived Neurons

(A) Representative control (clone G) and homozygous TFG (p.R106C)expressing (clone A) iPSC-derived cortical neurons were fixed and stained using antibodies directed against Sec31A (red), TFG (green), and Tau (white), and imaged using swept-field confocal optics. Maximum intensity projections are shown. Scale bars, 10 mm and 1 mm (insets).

(B) Representative control (clone G) and homozygous TFG (p.R106C)expressing (clone A) neurospheres were plated onto glass coverslips, and axon outgrowth was examined following fixation and staining using antibodies directed against Tau after 1 week. Maximum intensity projections are shown. Scale bar, 20 mm.

(C) Quantification of axon outgrowth observed in control (IMR90–4 and cloneG) and homozygous TFG (p.R106C)-expressing neurospheres (clones A, B, and C) 1 week after plating. Error bars represent mean ± SEM; n > 10 neurospheres per condition; three biological replicates each. No statistically significant difference was found, as calculated using a paired t test.

(D) Quantification of axon bundling in control (IMR90–4 and clone G), homozygous TFG (p.R106C)-expressing neurospheres (clones A, B, and C), and heterozygous SPG3A (p.P342S)-expressing neurospheres (16) 1 week after plating was calculated based on the ratio of axon thickness measured using linescan analysis at 150 mm from the edge of the neurosphere to the thickness measured 10 mm from the neurosphere. Error bars represent mean ± SEM; n > 10 neurospheres per condition; three biological replicates each. **p < 0.01, as calculated using an ANOVA test.

See also Figure S5 and S6.

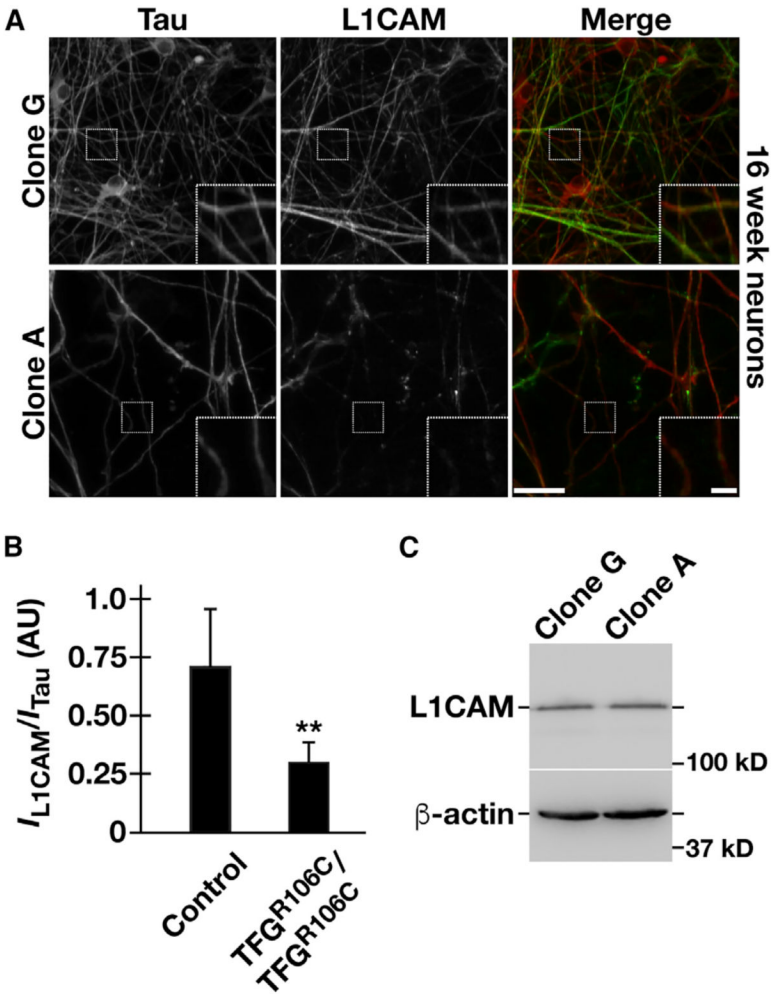

Figure 7. The TFG (p.R106C) Mutation Leads to a Defect in L1CAM Accumulation at the Surface of Axons in iPSC-Derived Neurons

(A) Representative control (clone G) and homozygous TFG (p.R106C)expressing (clone A) cortical neurons were grown for 16 weeks in culture and subsequently incubated live with antibodies directed against L1CAM (green). Neurons were then fixed and stained using antibodies directed against Tau (red). Maximum intensity projections are shown. Scale bars, 20 mm and 5 mm (insets).

(B) Fluorescence intensity (I) of L1CAM relative to Tau in axons from control(clone G) and homozygous TFG (p.R106C) mutant iPSC-derived neurons. Error bars represent mean ± SEM; n > 50 axons per condition; three biological replicates each. **p < 0.01 (compared with control), calculated using a paired t test.

(C) Representative immunoblot analysis of control iPSC-derived neurons(clone G) and neurons harboring the homozygous TFG (p.R106C) mutation (clone A) using antibodies directed against L1CAM and b-actin. Densitometry analysis was performed to quantify changes in L1CAM levels relative to b-actin in both control and homozygous TFG (p.R106C)-expressing iPSC-derived neurons (n = 3). No statistically significant difference was found, as calculated using a paired t test.

See also Figure S7.